Volume 10, Number 1 (February 2017) p. 53 - 83 • ISSN 1983-4195
http://dx.doi.org/10.1590/S1983-41952017000100004

REVISTA IBRACON DE ESTRUTURAS E MATERIAIS
IBRACON STRUCTURES AND MATERIALS JOURNAL

Numerical analysis of nonlinear behavior of steel concrete composite structures

Análise numérica do comportamento não linear de estruturas mistas de aço e concreto




Í. J. M. LEMES [a]
igorjml@hotmail.com

A. R. D. SILVA [a]
andreardsilva@em.ufop.br

R. A. M. SILVEIRA [a]
ricardo@em.ufop.br

P. A. S. ROCHA [b]
paulorocha@em.ufop.br

Abstract

This paper presents the development of an effective numerical formulation for analysis of steel concrete composite structures considering geometric and materials nonlinear effects. Thus, a methodology based on Refined Plastic Hinge Method (RPHM) was developed and the stiffness parameters obtained by homogenization of cross section. The evaluation of structural elements strength is done through the Strain Compatibility Method (SCM). The Newton-Raphson method with path-following strategies is adopted to solve nonlinear global and local (in cross section level) equations. The results are compared with experimental and numerical database presents in literature and a good accuracy is observed in composite cross section, columns and portal frames.

Keywords: nonlinear analysis, RPHM, interaction curves, SCM, moment-curvature relationship.

Resumo

O presente trabalho apresenta o desenvolvimento de uma formulação numérica adequada para análise de estruturas mistas de aço e concreto considerando os efeitos da não linearidade geométrica e da inelasticidade dos materiais. Para tal, foi desenvolvida uma metodologia baseada no Método da Rótula Plástica Refinado (MRPR), sendo os coeficientes de rigidez obtidos por meio da homogeneização da seção transversal. A avaliação da capacidade resistente dos elementos estruturais é feita no contexto do Método da Compatibilidade de Deformações (MCD). Os problemas oriundos da consideração das fontes de não linearidade (global e local) são resolvidos por meio do método iterativo de Newton--Raphson acoplado a estratégias de continuação. Os resultados obtidos são comparados com aqueles fornecidos em análises experimentais e/ou numéricas presentes na literatura, sendo verificada boa precisão nas análises de seções transversais mistas, pilares isolados mistos e pórticos simples mistos.

Palavras-chave: análise não linear, MRPR, curvas de interação, MCD, relação momento-curvatura.

[a] *Departamento de Engenharia Civil, Escola de Minas, Universidade Federal de Ouro Preto, Ouro Preto, Minas Gerais, Brasil.*

Received: 19 Dec 2015 • Accepted: 15 May 2016 • Available Online: 06 Feb 2017

1. Introduction

When considering the nonlinear behavior of structures, the approaches proposed by design codes become less realistic as the structural elements become slender. In the current context, the use of high-strength materials in construction gives rise to less rigid structures that are susceptible to large displacements. Accurate analysis of such structures requires the use of computational tools that take into account both the nonlinear behavior of the geometry of the structure and the bearing capacity of its structural elements. Structures made up of two or more materials are referred to as composite structures. The objective of this sort of combination is to find a balance between the materials, one that minimizes the unfavorable characteristics of each component. For example, concrete has been used only to protect steel against corrosion and fire agents, although it also happens to contribute to increasing the bearing capacity and stiffness of the structure. This idea spurred the first composite steel-concrete structural elements.

It is not at all simple to define the stiffness and bearing capacity of composite structural elements and the complexity is due to the concrete's anisotropic characteristics. Design codes [1-2] propose simplified methodologies for defining these stiffness parameters and full yield curve that can either approximate or hold off the actual behavior of the structure [3].

One alternative for obtaining accurate results in a way that is more computationally feasible is the Refined Plastic Hinge Method (RPHM). Usually the RPHM is associated with the analysis of steel [4-5] and composite structures [6-7]. In these approaches, the cross-section flexural stiffness is possibly degraded by pseudo-spring elements inserted in the ends of finite elements. The degradation begins when the combination of the axial force and the bending moment exceeds the limit of the elastic stage imposed by the initial yield curve. In other words, the cross-section maintains linear elastic behavior only up to the beginning of this curve.

When it comes to assessing the bearing capacity of the composite steel-concrete elements using Strain Compatibility Method (SCM) [2, 7], two strategies stand out. For nonlinear problems, proponents of quasi-Newton methods, such as Chen *et al.* [8] and Liu *et al.* [9], use this solution procedure, coupled with the Regula-Falsi numerical scheme. The process consists of determining the neutral axis position and its orientation (3D problem), which are the parameters set in the iterative cycle. In such manner, one can obtain the cross section bearing capacity. The Newton-Raphson method [10-11] uses, however, as the axial strain adjustment variables the membrane effect at the plastic centroid of the section and the curvature effect in one of the main axes (2D problem). The axial strain of each discrete point in the section is then determined and the respective constitutive relationships are used for the sum of stresses. The procedure consists of constructing the moment-curvature relationship (nonlinear problem), where, for a given axial force, the limit point that is found for the bending moment reflects the axial force-bending moment combination responsible for the plastification of the section. By analyzing moment-curvature the stiffness parameters can be determined. Chiorean [11] obtained the flexural rigidity of the section based on the tangent to the moment-curvature. Liu *et al.* [12] has already reduced the moment of inertia of reinforced concrete elements as cracking occurred. Furthermore, Chan *et al.* [13] used the homogenized stiffness section to calculate the coefficients of the stiffness matrix.

This work aims to couple the SCM to RPHM to provide the Computational System of Advanced Structural Analysis (CS-ASA) platform [7] a formulation that is capable of assessing the load carrying capacity of composite structures while considering both the effects of geometric and physical nonlinearities. It is a new formulation within the context of evaluating plasticity in a concentrated form. Thus, the formulation retains the simplicity and small computational effort of RPHM and takes into account the accuracy of the SCM in the evaluation of cross section bearing capacity. While some recent studies have similarly coupled RPHM and SCM, none of their analyses of the bearing capacity of the cross-section uses the construction of the moment-curvature relationship. Moreover, to expand the range of analysis possibilities, the study also implements prescriptive requirements [1-2] to obtain the load carrying capacity of the elements. This would make it possible to assess the structural behavior of composite elements based on design codes considerations and to compare results obtained using the generalized formulation proposed by coupling RPHM with SCM.

2. Fundamentals for nonlinear structural analysis

The global nonlinear structural problem in the context of the Finite Element Method (FEM) and RPHM/SCM, is resolved by the following equation:

$$\mathbf{F}_i\left(\mathbf{U},\mathbf{P},S\right)\cong\lambda\mathbf{F}_r \qquad (1)$$

with $\mathbf{F}_i$ the internal force vector, which is written on the basis of nodal displacement vector $\mathbf{U}$, internal forces in members, $\mathbf{P}$, and the evaluation parameter of the flexural section stiffness degradation , S. The external forces vector is defined by the product between the load parameter, λ, and $\mathbf{F}_r$, which is the external forces vector of reference.

Equation (1) is solved here by the Newton-Raphson method used in conjunction with path-following strategies, such as the generalized displacement technique [14] and the minimum residual displacements method [15].

Computationally, the effects of geometric nonlinearity are introduced in the conventional stiffness matrix by the matrix $\mathbf{K}_\sigma$, $\mathbf{K}_1$ and $\mathbf{K}_2$. $\mathbf{K}_\sigma$ is the geometric stiffness matrix, $\mathbf{K}_1$ is a linear function of the incremental nodal displacements while the terms in the matrix $\mathbf{K}_2$ are quadratic functions [16]. Terms of higher order ($\mathbf{K}_1$ and $\mathbf{K}_2$) can be neglected, especially when the structures are rigid and the material nonlinearity is more relevant.

3. Concentrated plasticity analysis

The computer program CS-ASA [5] has been under development since 2009 and has already been established for the nonlinear analysis of steel structures. This program uses the Refined Plastic Hinge Method (RPHM) [4] to simulate the concentrated plasticity in the nodal points.

To model the structures considered in this work, the study adopts the following assumptions:

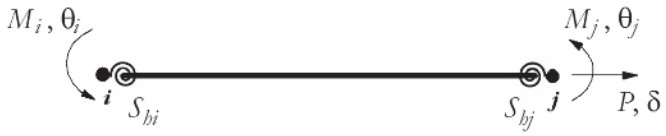

Figure 1
Hybrid finite element with section springs

- there is full interaction between the materials present in the cross-section;
- the elements are initially straight, prismatic, and warpage may be ignored;
- the structure is perfectly locked on to the orthogonal axis (2D problem);
- effects of localized instability are neglected;
- large displacements and rigid body rotations are allowed;
- shear strain effects are neglected.

In the modeling, the beam-column finite element used is shown in Fig. 1. This element is defined by the nodes *i* and *j*. Also illustrated are the internal forces, M_i, M_j and P, as well as their respective degrees of freedom θ_i, θ_j and δ, referenced to the corrotational system. Null length pseudo-springs are inserted, at the ends of the element, to simulate the degradation of flexural stiffness by parameter *S*.

The *S* parameter is set within three domains (Fig. 2). When in the elastic state, the value of *S* is assumed to be 10^{16}. Such a state is limited by the beginning of initial yield curve. Upon reaching the plastic state (a situation where the internal forces reach the full yield curve), the flexural stiffness is completely degraded. In this case, *S* is taken to be numerically equal to 10^{-10}. Between the initial and full yield curves, the loss of stiffness is considered to occur gradually, according to the following equation:

$$S = \frac{(EI)_{comp}}{L}\left(\frac{M_{pr} - M}{M - M_{er}}\right) \qquad (2)$$

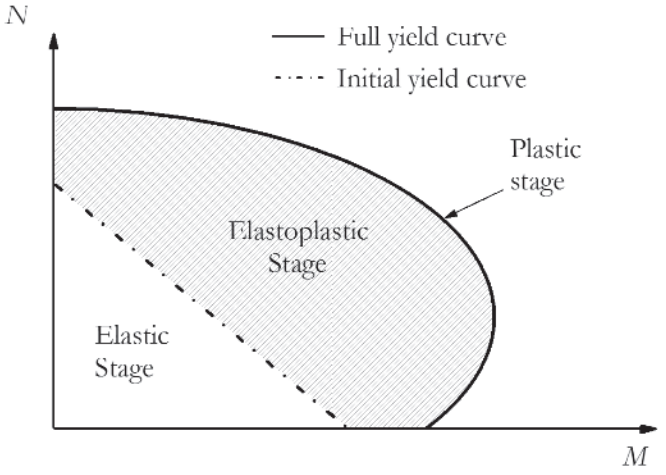

Figure 2
Full and initial yield curves: pseudo-spring flexural stiffness definition

where *L* is the length of the finite element; M_{pr} is the full yield moment and M_{er} the initial yield moment, which will be defined in Section 4; and $(EI)_{comp}$ is the flexural stiffness of the homogenized composite section that, for doubly symmetrical and composite beams section, is given by [17]:

$$(EI)_{comp} = \eta\left[(EI)_a + (EI)_b + (\mu EI)_c\right] \qquad (3a)$$

$$(EI)_{comp} = E_a\left(0,4\,I_{comp} + 0,6\,I'_{comp}\right) \qquad (3b)$$

where the subscripts *a*, *b*, and *c* refer to steel section, the reinforcement bar, and concrete; μ is the reduction factor for the flexural stiffness of concrete due to cracking; η is a reducing of the global stiffness coefficient; and I_{comp} and I'_{comp} are the moments of inertia of the composite section in the positive and negative moment regions, respectively.

For the element shown in Fig. 1, the force-displacement relationship is expressed by [9]:

$$\begin{Bmatrix}\Delta P\\ \Delta M_i\\ \Delta M_j\end{Bmatrix} = \begin{bmatrix} EA_{comp}/L & 0 & 0\\ 0 & S_i - S_i^2\left(k_{jj} + S_j\right)/\beta & \left(S_i S_j k_{ij}\right)/\beta\\ 0 & \left(S_i S_j k_{ji}\right)/\beta & S_j - S_j^2\left(k_{ii} + S_i\right)/\beta\end{bmatrix}\begin{Bmatrix}\Delta\delta\\ \Delta\theta_i\\ \Delta\theta_j\end{Bmatrix} \qquad (4)$$

or

$$\Delta\mathbf{f}_{co} = \mathbf{K}_{co}\Delta\mathbf{u}_{co}$$

with $\beta = (S_i + k_{ii})(S_j + k_{jj}) - k_{ji}k_{ij}$. The subscripts *i* and *j* indicate the nodes of the element and *co* the subscript to the coordinate system used (corrotational); $(EA)_{comp}$ is the axial stiffness of the homogenized cross-section; ΔP and ΔM are, respectively, the incremental axial force and bending moment; $\Delta\delta$ and $\Delta\theta$ are the increments of axial strain and nodal rotation.

The terms k_{ii}, k_{ij}, k_{ji} and k_{jj} are obtained according to the Yang and Kuo's formulation [14]. When the section plastify, any increase in incremental load causes the internal forces to extrapolate the full yield curve, therefore, violating the cross-section bearing capacity. The formulation used here avoiding this violation is a strategy known as Return Mapping [5]. In this strategy, the element axial force remains constant and returns the internal bending moment to the full yield curve. In other words, Eq. (4) is modified so that in these situations the bearing capacity of the elements is not violated.

4. Strain compatibility method

The bending moments M_{pr} and M_{er}, used in Eq. (2), are obtained in the context of the Strain Compatibility Method (SCM). Compared to the simplified design codes procedures [1, 2], a more realistic approach is produced by the coupling of the deformed shape of section and the constitutive relationships of the materials comprising it. To satisfactorily obtain the strain field in the section, the cross-section discretization is necessary. In the discretization, the strength may be sufficiently evaluated with two-dimensional layers, but this procedure is sensitive to the degree of refinement imposed by the analyst.

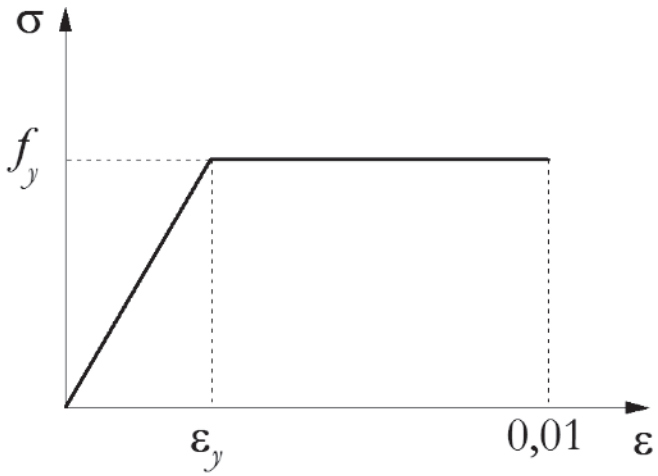

Figure 3
Steel constitutive relationship

4.1 Steel behavior

Fong and Chan [6] proposed for both the reinforcing bars and for the steel section an elastic-perfectly-plastic constitutive relationship (shown in Fig. 3), as described below:

$$\sigma \begin{cases} -f_y & \text{if} -\varepsilon_u \le \varepsilon \le -\varepsilon_y \\ E_a \varepsilon & \text{if } -\varepsilon_y < \varepsilon < \varepsilon_y \\ f_y & \text{if } \varepsilon_y \le \varepsilon \le \varepsilon_u \end{cases} \quad (5)$$

where f_y is the yield strength of steel, E_a the Young's modulus of steel, ε_y and ε_u the elastic limit and final limit of steel strains, respectively.

4.2 Concrete behavior

When compressed, the parabolic-rectangular stress-strains relationship is adopted (Fig. 4a), limited by the last of the concrete compressive strain, ε_{cu}. As proposed by Bazant and Oh [18], it is also possible to consider the tensile strength given by a bilinear model with a positive slope until reaching the beginning of cracking strain, ε_{tr}, along with the ultimate tensile strength, f_{cr} (Fig. 4b). The strain limit to the tensioned concrete is considered here as 0.0007, adopted by Bratina *et al.* [19]. We thus have:

$$\sigma = \begin{cases} -f_c & \text{if } \varepsilon_{cu} \le \varepsilon \le \varepsilon_{ci} \\ \left[\dfrac{2\varepsilon}{\varepsilon_{ci}} - \left(\dfrac{\varepsilon}{\varepsilon_{ci}} \right)^2 \right] f_c & \text{if } \varepsilon_{ci} < \varepsilon \le 0 \\ E_{tr}\varepsilon & \text{if } 0 \le \varepsilon \le \varepsilon_{cr} \\ E_{tr,2}\left(\varepsilon - \varepsilon_{cr}\right) & \text{if } 0{,}0007 \ge \varepsilon > \varepsilon_{cr} \end{cases} \quad (6)$$

where f_c is the maximum compression strength of concrete, E_{tr} and $E_{tr,2}$ are the concrete modulus of elasticity in tension, before and after cracking. ε_{ci} is the strain limit of the parabolic curve of the compressed concrete.

4.3 Moment-curvature relationship

Once the cross-section is discretized, in using the SCM coupled with the Newton-Raphson Method, there are two relevant variables: the area of the layers and their respective positions. This second is referred to as the plastic centroid (PC), so as to minimize convergence problems [8].
The position of the PC section is obtained by the following expression [20]:

$$y_{cp} = \frac{y_c A_c \gamma f_{cd} + y_a A_a f_{yd} + y_b A_b f_{ybd}}{A_c \gamma f_{cd} + A_a f_{yd} + A_b f_{ybd}} \quad (7)$$

with A_c, A_a and A_b being the concrete, steel, and the reinforcing bars areas; γ is the confinement coefficient of concrete; y_c, y_a and y_b are the coordinates of the respective areas' centroids

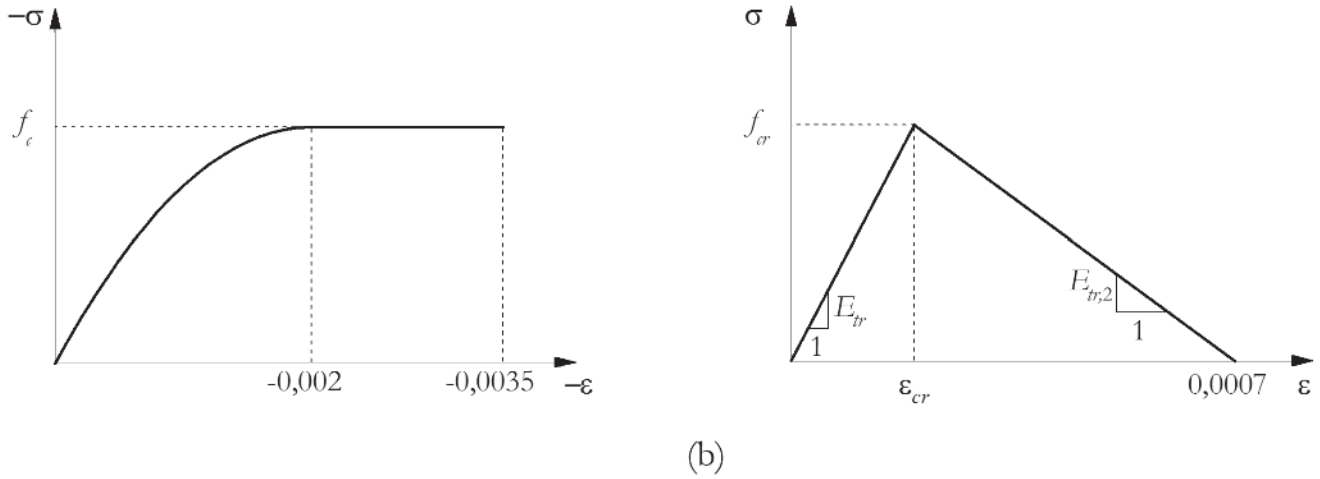

(a) (b)

Figure 4
Concrete constitutive relationship (a) compression and (b) tensile

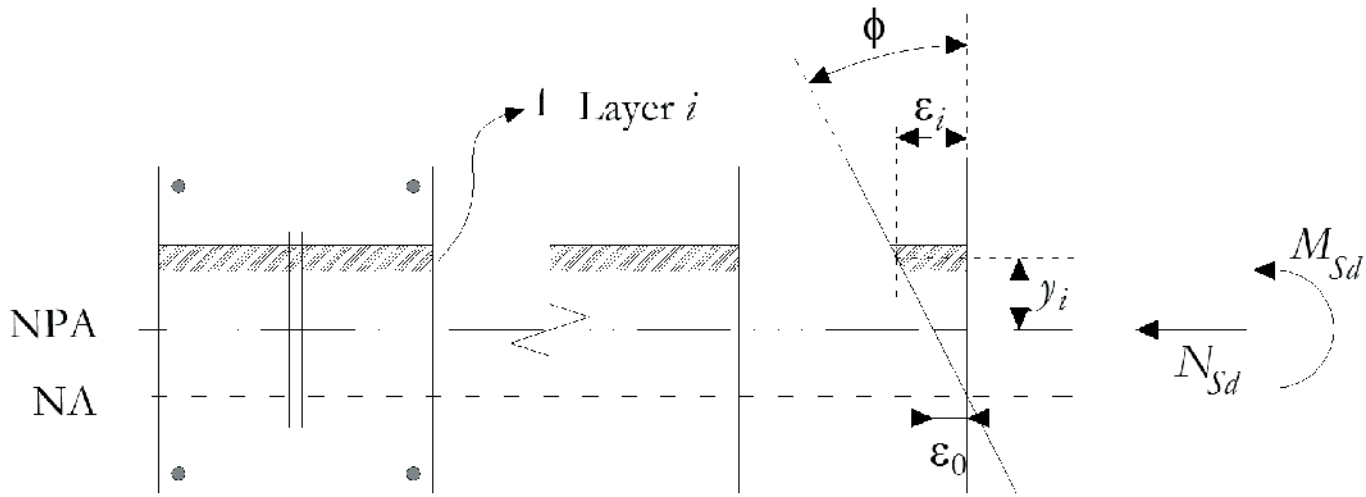

Figure 5
2D linear strain field

on the ordinate axis in relation to a reference system; and f_{cd}, f_{yd} and f_{ybd} are the compressed concrete, steel and reinforcing bars strength, respectively.

Figure 5 illustrates the distribution of strains in the composite section from a combination of axial force and bending moment. Note that the total axial strain at the i^{th} slice, ε_i, is given by a linear function. Therefore:

$$\varepsilon_i = \varepsilon_0 + \phi\, y_i \tag{8}$$

where y_i is the distance between the of the analyzed layer and the cross-section plastic centroids (PCs), ε_0 is the membrane strain in the section CP, and ϕ its curvature.

For the matrix notation, the study adopted the following: the variables ε_0 and ϕ are the positions of the strain vector $\mathbf{X} = [\varepsilon_0 \;\; \phi]^T$. It is necessary to adjust the vector **X** until the deformed shape of the section is consistent with the active external forces. This adjustment is made through the iterative process described below. Chiorean [11] pointed out that adopting **X** = **0** in the first iteration enables a faster convergence. Numerically, it can be said that the balance of the section is obtained when the following equation is satisfied:

$$\mathbf{F}(\mathbf{X}) = \mathbf{f}_{ext} - \mathbf{f}_{int} \cong 0 \tag{9}$$

where the external forces vector is depicted as $\mathbf{f}_{ext} = [\mathrm{N} \;\; \mathrm{M}]^T$.

But the internal force vector is given by classical integral expressions for the axial force, N_{int}, and bending moment, M_{int}. Once areas, A_i, and positions, y_i, of each layer are known, the integral becomes the sum described as:

$$\mathrm{f_{int}} = \begin{bmatrix} \sum_{i=1}^{n_{fat}} \sigma_{ai}A_{ai} + \sum_{i=1}^{n_{fat}} \sigma_{ci}A_{ci} + \sum_{j=1}^{n_b} \sigma_{bj}A_{bj} - \sum_{j=1}^{n_b} \sigma_{cj}A_{cj} \\ \sum_{i=1}^{n_{fat}} \sigma_{ai}A_{ai}y_{ai} + \sum_{i=1}^{n_{fat}} \sigma_{ci}A_{ci}y_{ci} + \sum_{j=1}^{n_b} \sigma_{bj}A_{bj}y_{bj} - \sum_{j=1}^{n_b} \sigma_{cj}A_{cj}y_{cj} \end{bmatrix} \tag{10}$$

with n_{fat} being the number of layers used in the discretization of the cross-section and n_b the number of reinforcing bars lines present in the composite section. Layers stresses, σ, are dependent on the deformed shape of the cross-section, and are therefore functions of ε_0 and ϕ.

While it is appropriate to initiate the process with **X** = **0**, convergence is achieved only in the first iteration if external forces are null. Thus, for the next iteration, k+1, the strain vector is given by:

$$\mathbf{X}^{k+1} = \mathbf{X}^k + \mathbf{F}'\left(\mathbf{X}^k\right)^{-1}\mathbf{F}\left(\mathbf{X}^k\right) \tag{11}$$

where **F**' is the tangent stiffness matrix of the cross-section or the Jacobian matrix of the nonlinear problem stated in Eq. (9), that is:

$$\mathbf{F}' = \left(\frac{\partial \mathbf{F}}{\partial \mathbf{X}}\right) = \begin{bmatrix} \frac{\partial N_{int}}{\partial \varepsilon_0} & \frac{\partial N_{int}}{\partial \phi} \\ \frac{\partial M_{int}}{\partial \varepsilon_0} & \frac{\partial M_{int}}{\partial \phi} \end{bmatrix} \tag{12}$$

The convergence criterion adopted in this work is based on the ratio of the Euclidean norms of the unbalanced force vector, **F**, and the external forces vector, $\mathbf{f}_{ext}$. Thus, this ratio should be less than a tolerance, assumed here to be 10^{-5}.

Figure 6 details the flow chart of the process for obtaining the moment-curvature relationship.

When, for a given axial force, the maximum bending moment of the moment-curvature is reached, there is a total plastification of the section. It is defined such that a pair of forces is a point on the full yield curve.

The initial yield curve also is obtained from the moment-curvature relation. When the first layer of the section presents axial strain, ε, greater than the yield strain of the steel (section or longitudinal reinforcing bars) and/or the strain of the concrete's initial plastification [6], the layer begins to degrade and consequently the section loses stiffness. The moment responsible for this fact is considered the initial yield moment.

5. Limitations of the analysis methodology

In addition to the simplifying assumptions mentioned in Section 3, such as the full interaction between the materials, the disregard of shear strain, and so forth, there are some limitations in the proposed analysis methodology. The use of pseudo-springs at the ends of the finite element model to simulate the plasticity leads to a simplification consistent with the behavior of steel structures. In Figure 2, it can be seen that the rotational stiffness of the springs, discussed in Section 3, is defined within three domains (elastic, elastoplastic and plastic). Once within the elastic state, the *S* parameter of the pseudo-spring is kept constant, i.e., regardless the materials used in the structure, there is linear elastic behavior. This characterizes the linear behavior of the steel in Hooke's Law, shown in Fig. 3, for strains smaller than ε_y. Thus for the numerical simulation of composite structures in this formulation, the axial and flexural stiffness are evaluated by homogenizing the cross-section.

A more careful evaluation is called for in the study and analysis of reinforced concrete structures. As illustrated in Fig. 4, the concrete exhibits nonlinea r behavior under compression from strains smaller than ε_{ci}, which means a limitation to the use of pseudo-springs.

6. Numerical examples

The numerical strategies presented in previous sections are used now to aim at a nonlinear analysis of steel-concrete composite structural systems. Evaluated examples are divided into four groups: interaction curves, isolated concrete-filled steel columns, rectangular concrete-filled tube made of high-strength materials and simple composite portal frame. The results are compared with those reported in the literature, obtained numerically and/or experimentally. To simulate the following examples, we used a computer equipped with an Intel Core i7 2.20 GHz and 8 GB of RAM.

6.1 Full yield curves

This section looks at the full yield curves of two steel-concrete composite cross-sections. At first, the encased I section, shown in

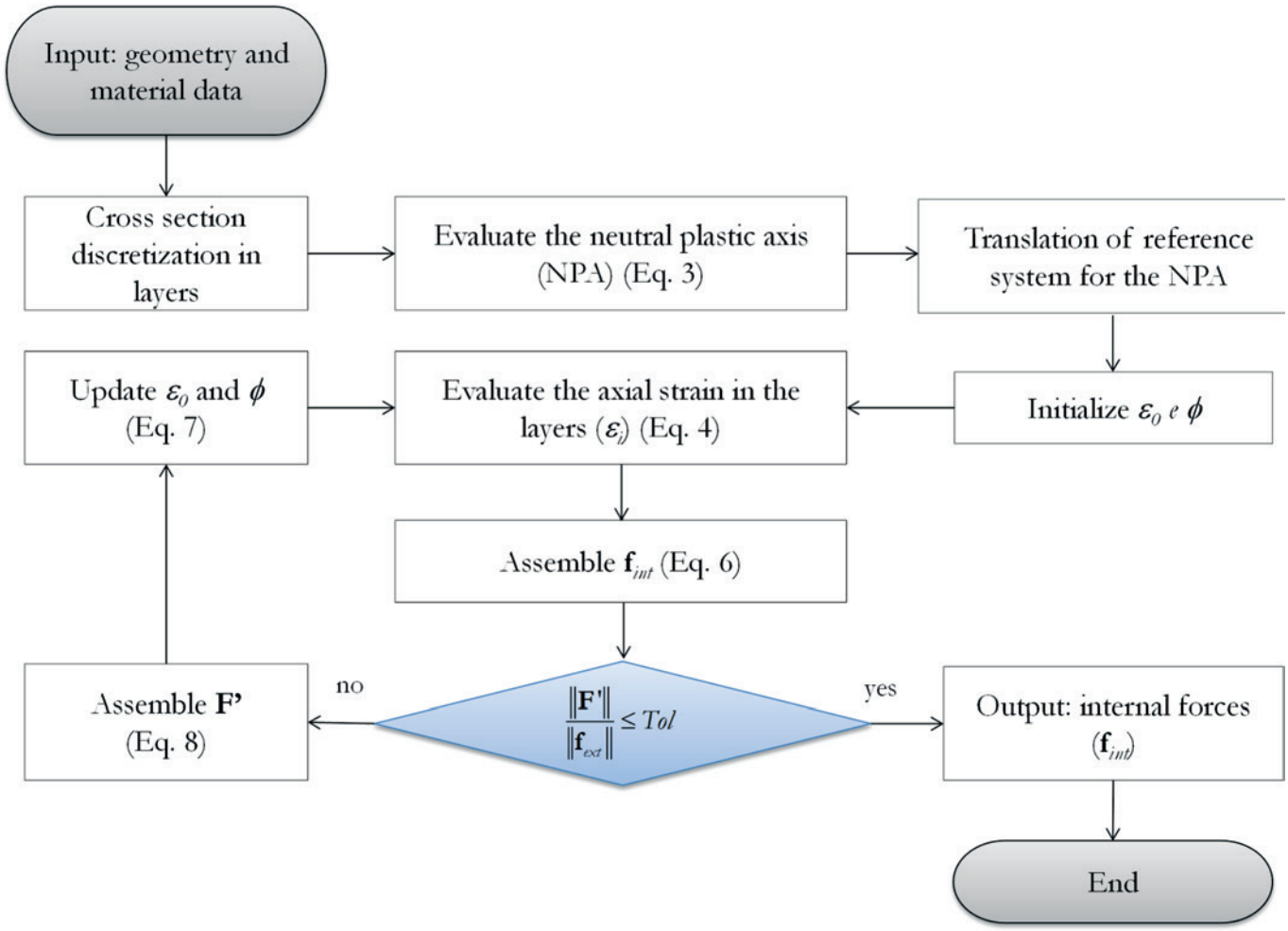

Figure 6
Nonlinear local problem solver – moment-curvature relationship

Fig. 7, is evaluated around the major and minor axes. It is a steel I section (256 x 256 x 14.4 x 16 mm), where f_y is taken to be equal to 250 MPa, completely encased by concrete with f_{ck} 25 MPa. Further, the steel circular section is studied; its outside diameter is 400 mm; it is 10 mm thick with f_y = 275 MPa filled with concrete with f_{ck} of 35 MPa. In each case, two analyses will be made: a CST analysis of the concrete will not have tensile strength; and a CCT analysis in which the constitutive relationship shown in Fig. 4b will be considered.

Interaction curves were constructed of 101 coordinate points (M, N), each of the sections discretized into 12 layers. Such data are presented in order to standardize comparative measures of runtime, which at that point were not provided in the literature.

Figure 7 shows the full yield curves of the encased I section to major and minor axes. The study also evaluated the increase of the cross-section bearing capacity while considering the tensile behavior of concrete, as shown in Fig. 4b. Numerically, this increase is approximately 2.1% in the first quadrant of the axial force-moment bending diagram. To construct the four curves, CSASA software took 0.57 seconds or 0.14 seconds, on average, to build each curve.

Figure 8 shows the bearing capacity behavior of a circular steel section filled with concrete. Once the section exhibited the same behavior in both the *x* and *y* axes, only one of the curves was plotted. In this case, that took 0.28 seconds, averaging 0.14 seconds for each curve. There was a 1.7% increase in bearing capacity in the first quadrant when considering the tensioned concrete contribution in the obtaining curve.

In the cases covered in this item, there was good agreement between the results obtained by the Newton-Raphson Method and those provided by Caldas [10], who constructed the curve using

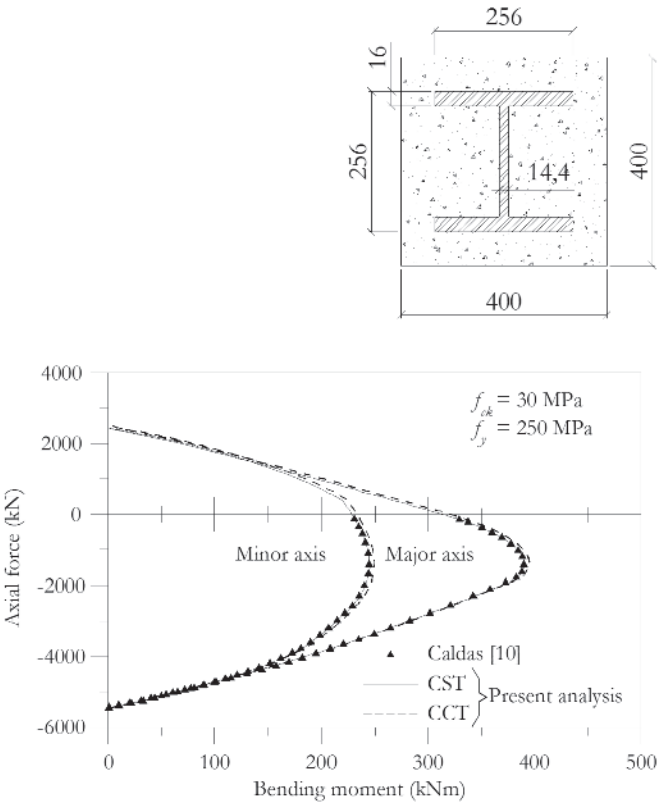

Figure 7
Full yield curves for encased I section

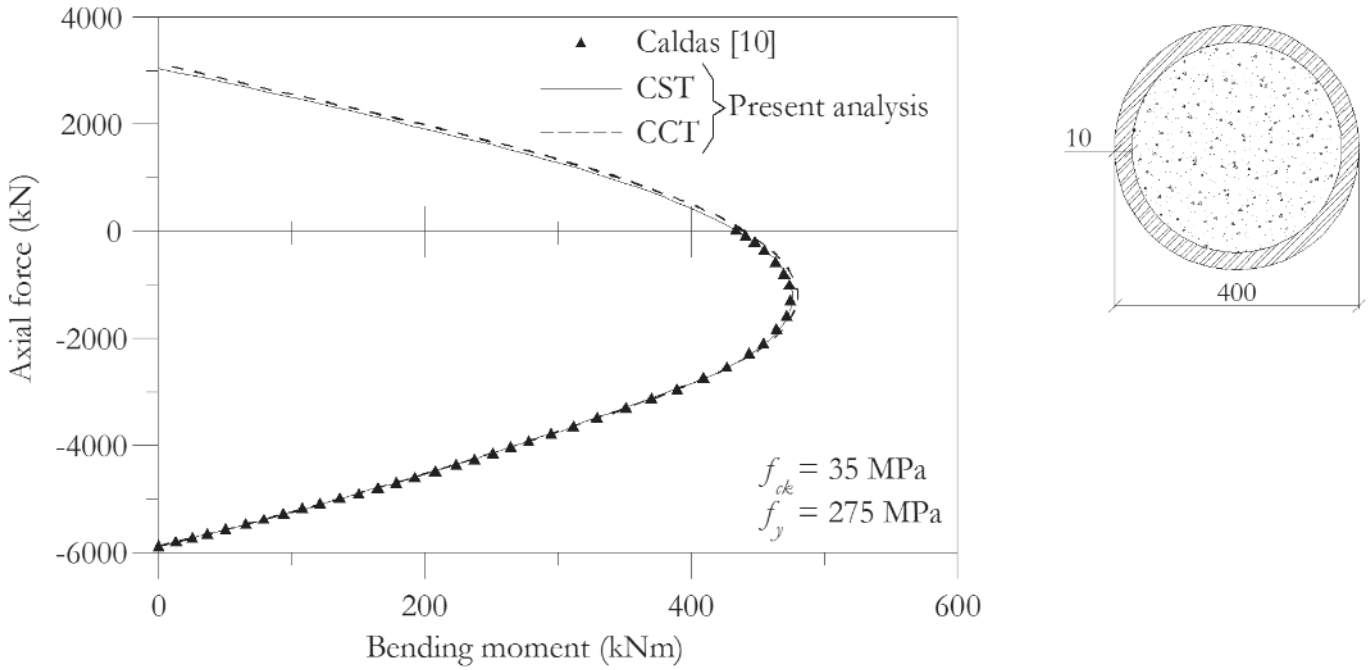

Figure 8
Full yield curve for circular composite section

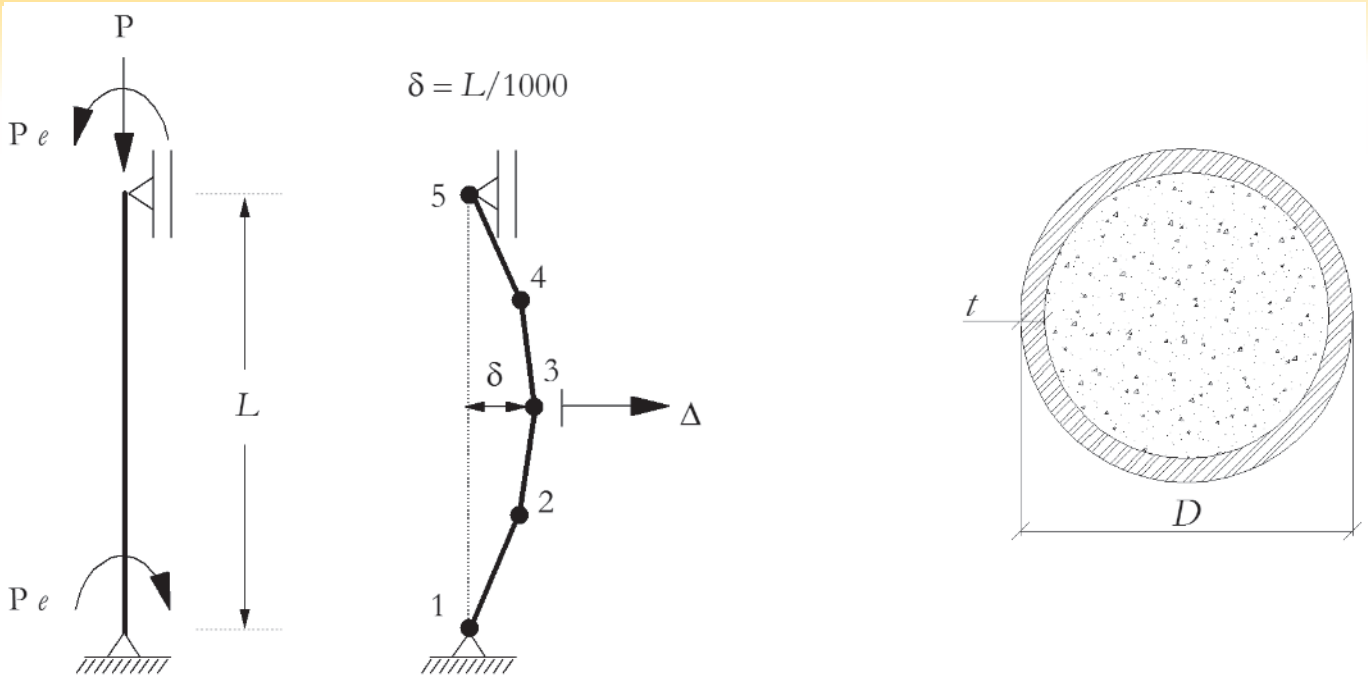

Figure 9
Idealized model for circular composite column with eccentric load analysis

the D-strain parameter approach. In this method, one of the strain parameters is taken from the concrete strain domains, and the equations are thus adjusted to cycle through the deformed shapes for the ultimate limit state of the section. In both cases discussed in this item, the proposal to adopt the singularity condition of the Jacobian matrix of the cross-section (Eq. 12) as a stopping criterion for the construction of the moment-curvature relationship is verified as being appropriate.

6.2 Concrete-filled steel columns

Seven concrete-filled steel circular columns were first experimentally analyzed by Neogi *et al.* [21]. Liu *et al.* [12] and Fong and Chan [6] used these experimental results to test their formulations based on RPHM. The simulated model consists of a column simply supported with an initial geometric imperfection (δ=*L*/1000). A load eccentricity is introduced to the system considering bending moments at both the top and base of the column, as shown in Fig. 9. To discretize the structural system, four finite elements are used. In local level, the circular cross-section was divided into 16 layers.

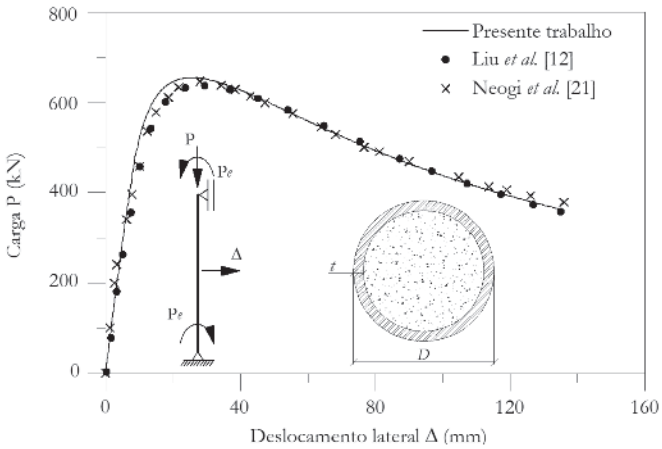

Figure 10
Equilibrium path – Column M5

Table 1
Geometry and material data

Specimen	L (mm)	e (mm)	D (mm)	t (mm)	f_y (kN/mm²)	f_{cu} (kN/mm²)
M1	3048	47,6	169,4	5,11	0,309	0,05553
M2	3048	38,1	169,2	5,26	0,309	0,054
M3	3048	47,6	168,9	5,66	0,295	0,04247
M4	3048	47,6	168,4	6,55	0,298	0,038
M5	3048	47,6	169,4	7,19	0,312	0,032
M6	3048	38,1	169,4	7,29	0,312	0,03318
M7	3022,6	47,6	168,9	8,81	0,323	0,03306

Table 2
Critical loads (kN), obtained using SCM and comparisons with the literature results

Specimen	P_{Test}	P_{Liu}	P_{CS}	Analysis time (s)	P_{CS}/P_{Test}	P_{CS}/P_{Liu}
M1	622	607,3	628,5	2,22	1,010	1,035
M2	702	695,1	698,7	2,65	0,995	1,005
M3	600	590,1	586,5	2,30	0,978	0,994
M4	625	621,3	628,3	2,31	1,005	1,011
M5	653	642,8	655,3	2,57	1,003	1,019
M6	739	732,9	733,9	2,79	0,993	1,001
M7	758	756,1	750,7	3,13	0,990	0,993
				Average	0,996	1,008
				Standard variation	0,0107	0,0149

For the load increase strategy [14], the first increase should be given and taken in this example as 2 kN.

The properties of the analyzed columns are shown in Table 1. The Young's modulus of steel is taken to be equal to 207000 MPa for all specimens. According to Liu *et al.* [12], Neogi *et al.* [21] did not provide the modulus of elasticity for concrete, so it is defined according to the ACI-318 recommendations [22].

Figure 10 offers a comparison of the equilibrium path for Column M5 obtained with the CS-ASA, provided by the Neogi *et al.* [21] and Liu *et al.* [12]. It can be observed in this same figure that there exists a slight difference at the beginning of the equilibrium paths — the simulated model CS-ASA appears slightly stiffer. Such divergence may be caused by the following sources: the geometric nonlinear formulation, the global and local refinements, plus some variables such as strain limits of the constitutive relationships of materials. After the load limit point is reached, the equilibrium paths are nearly the same.

Table 2 presents the critical loads attained in each of the simulations. The table also compares the values of the loads obtained here with those found in the literature. Compared to the experimental results, the low average difference, P_{Test} (0.4%), points to the reliability of numerical analyses presented for circular composite columns under axial force and bending moment. It is noteworthy that little difference is found when compared with the numerical results obtained by Liu *et al.* [12], P_{Liu}. Note that in Table 2, the value of the load limit obtained with the CS-ASA is denoted as P_{CS}. Another point to be highlighted in the formulation proposed in this paper, also shown in Table 2, is the low program runtime for the calculation of each of the prototypes. The time shown in the table reflects the time from the moment when the analysis began to the moment when the load limit point had been reached.

6.3 Rectangular concrete-filled tube made of high-strength materials

Liu *et al.* [23] conducted experimental tests on 21 rectangular concrete-filled tubes specimens. The materials used were high-strength — steel with an f_y equal to 550 MPa. The cylindrical

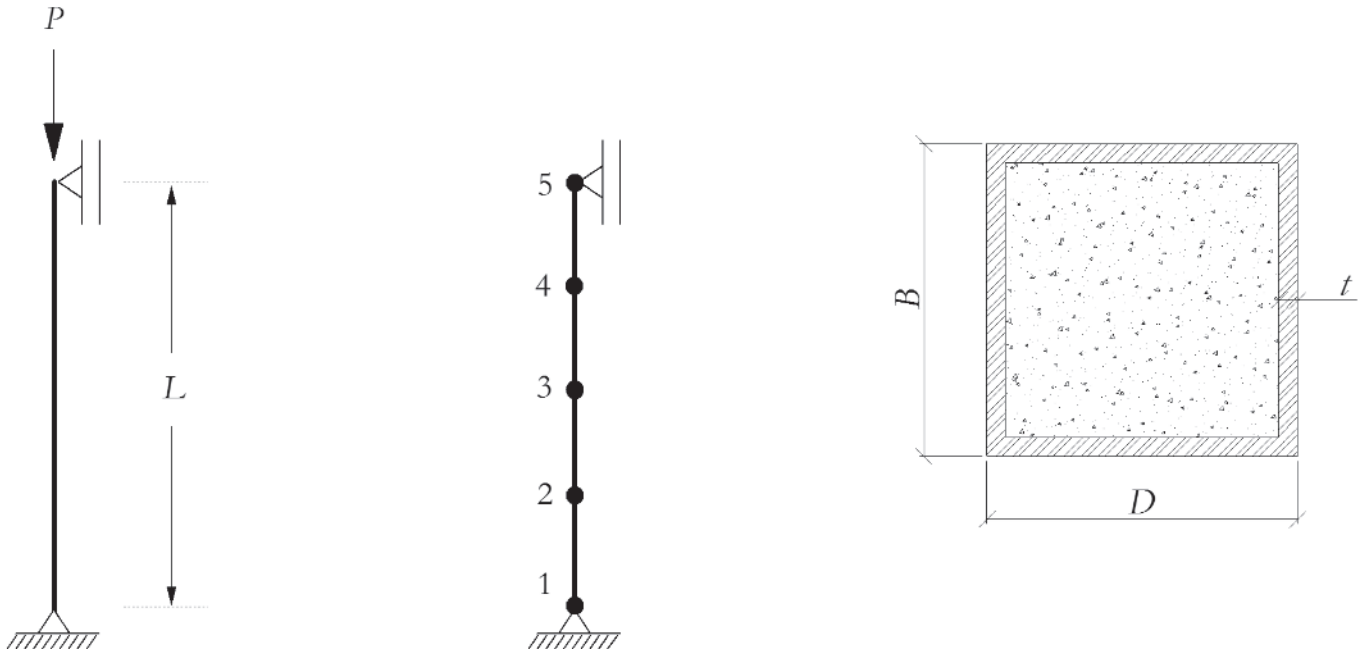

Figure 11
Idealized model for tubular rectangular composite column analysis

compressive strength of the concrete varied between 70.8 and 82.1 MPa. Basically, the tests were carried out using short columns so as to enable the cross-sections to have maximum load carrying capacity. Moreover, to prevent the occurrence of bending moments, the axial load on the structural element was applied concentrically. As illustrated in Fig. 11, the columns were simply supported and discretized in the same way at the global level, using four elements and five nodes, as at the local level, with 8 layers.

Table 3 presents the data of the cross-section and the results obtained with the formulation presented (P_{CS}). The table also compares the experimental results (P_{test}) with those obtained by Liu *et al.* [23]. The table shows a good approximation between the numerical and experimental results. On average, the data extracted from the CS-ASA program varies from the data obtained in the laboratory by only 1.9%. Also noteworthy, shown by the standard variation, is how low the dispersion of results are compared to the calculated average. Such a pattern demonstrates the numerical formulation's reliability. The table also shows the program execution times for each of the simulated specimens.

Regardless of considering the geometric nonlinearity, the critical load of the column is defined solely by the full yield curve. This occurs because the column is classified as short, i.e., it has low slenderness. Another conditioning factor is the position of the load application in the section's centroid, which makes the column be under the action of axial loading without bending moments. In other words, the limit load on the columns is equal to the point on the interaction curve where there is maximum compressive normal force and the bending moment is null.

Note that in some cases where two specimens were made of the same materials, the specimen with a smaller cross-section showed, in experimental terms, a load limit higher than that of the other element tested. This can be seen when comparing the C2-1 and C2-2 specimens. Theoretically, these values should be inverted, since the reduction of the cross-section directly implies a reduction in the bearing capacity of the structural element. In the

Table 3
Cross-section data and critical loads

Specimen	B (mm)	h (mm)	t (mm)	L (mm)	P_{Test} (kN)	P_{CS} (kN)	Analysis time (s)	$\frac{P_{CS}}{P_{Test}}$
C1-1	**100,3**	**98,2**	**4,18**	**300**	**1490**	**1459**	**1,25**	**0,979**
C1-2	**101,5**	**100,6**	**4,18**	**300**	**1535**	**1500**	**1,31**	**0,977**
C2-1	101,2	101,1	4,18	300	1740	1599	1,53	0,919
C2-2	100,7	100,4	4,18	300	1775	1585	1,36	0,893
C3	182,8	181,2	4,18	540	3590	3469	2,43	0,966
C4	181,8	180,4	4,18	540	4210	4078	2,94	0,969
C5-1	120,7	80,1	4,18	360	1450	1455	1,37	1,003
C5-2	119,3	80,6	4,18	360	1425	1449	1,39	1,017
C6-1	**119,6**	**80,6**	**4,18**	**360**	**1560**	**1542**	**1,43**	**0,988**
C6-2	**120,5**	**80,6**	**4,18**	**360**	**1700**	**1552**	**1,33**	**0,913**
C7-1	179,7	121,5	4,18	540	2530	2526	2,07	0,998
C8-1	**180,4**	**119,8**	**4,18**	**540**	**2970**	**2917**	**2,30**	**0,982**
C8-2	**179,2**	**121,3**	**4,18**	**540**	**2590**	**2928**	**2,33**	**1,131**
C9-1	160,2	81,4	4,18	480	1710	1747	1,60	1,022
C9-2	160,7	80,5	4,18	480	1820	1739	1,59	0,955
C10-1	160,1	81,0	4,18	480	1880	1865	1,62	0,992
C10-2	160,6	80,1	4,18	480	2100	1856	1,65	0,884
C11-1	199,8	101,2	4,18	600	2350	2426	1,97	1,032
C11-2	200,2	98,9	4,18	600	2380	2411	1,97	1,013
C12-1	199,2	102,1	4,18	600	2900	2816	2,23	0,971
C12-2	199,8	99,6	4,18	600	2800	2773	2,03	0,990
							Average	0,981
							Standard variation	0,053

C6-1 and C6-2 columns, it can be seen that, in testing the slightly larger section (C6-2), it had a 9% higher load capacity. Finally, we highlight the results of the C8-1 and C8-2 columns. These columns of very similar sections and of the same materials demonstrated a 15% difference in bearing capacities. In such cited cases, one sees the greatest discrepancy confronted the experimental results of these columns with analyses via CS-ASA.

6.4 Simple frames

The simple frame shown in Fig. 12 was initially presented by Liew *et al.* [17] in a study of steel structural systems with composite beams. Comparing it with a steel system, the authors studied how including a concrete slab impacted the gain in stiffness and load carrying capacity provided. Iu *et al.* [24] had already proposed fully coating the columns with concrete. Later, Chiorean [11] validated his formulation when he compared his load-displacement curves with those found in the literature.

The structure in question is a simple frame with a height and width of 5 m, the columns having a W12 x 50 section and the beam a W12 x 27 section. As for the concrete slab, its height is 102 mm and its width 1219 mm. The columns are encased in the second

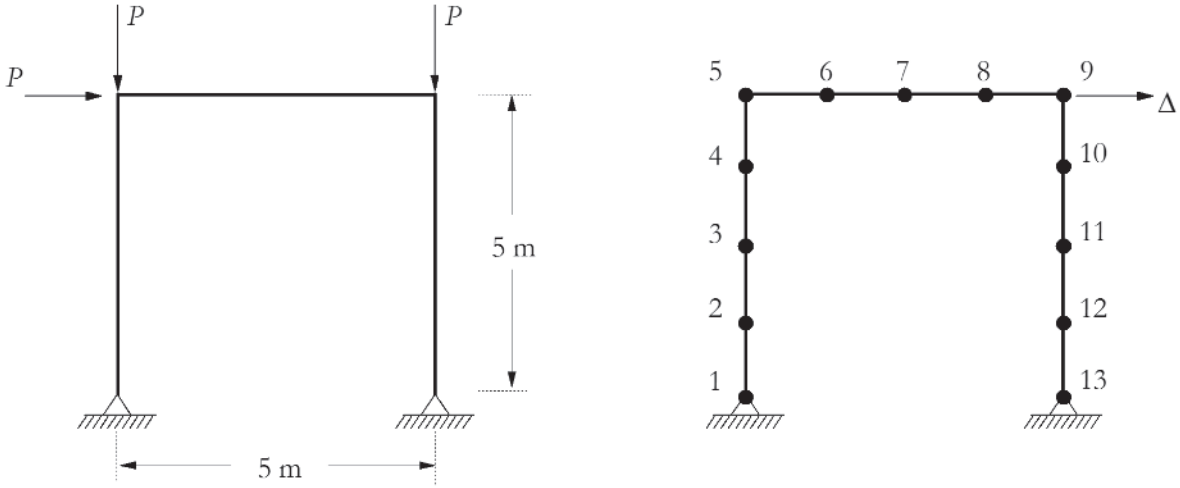

(a) Geometry, loads and adopted discretization

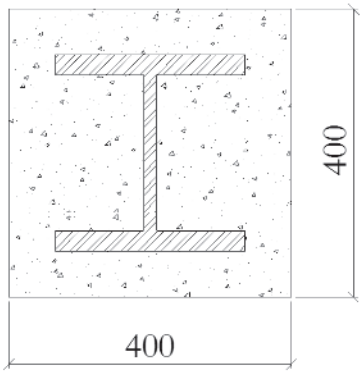

(b) Cross-section of encased I section

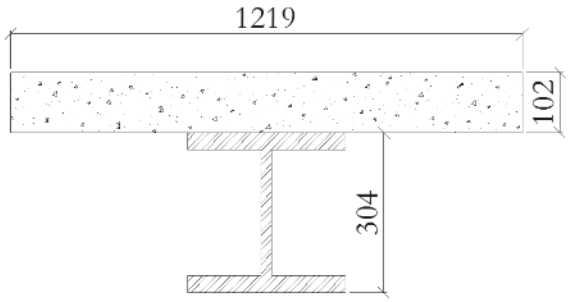

(c) Cross-section of composite beam

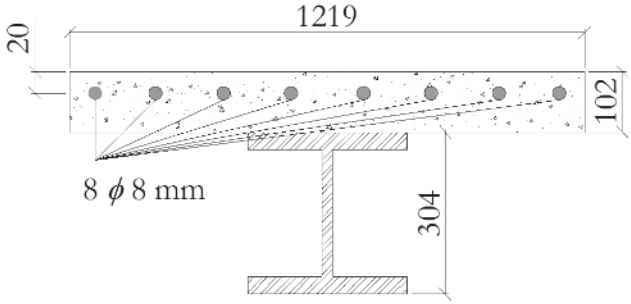

(d) Cross-section of reinforced beam – Structures 3 e 4

Figure 12
Simple frame

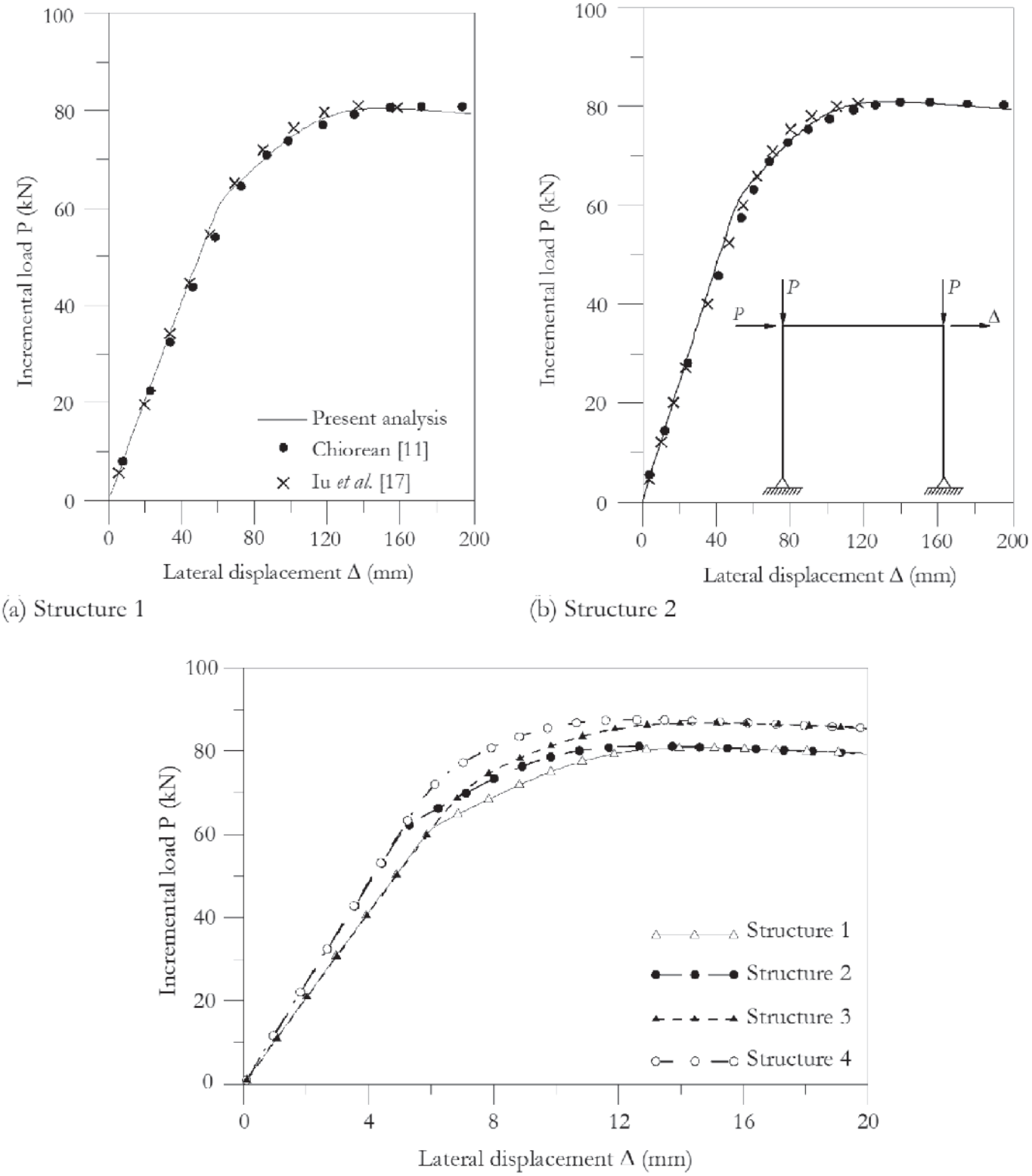

(a) Structure 1

(b) Structure 2

(c) Comparison of four numerically simulated structures

Figure 13
Simple frame: equilibrium paths

analysis, making for a square composite section with a base equal to 400 mm (Fig. 12b). Vertical incremental loads were applied to the tops of the columns, and a horizontal load to the top of the left column. The frame was considered to have no initial geometric imperfections. Each frame member was divided into four finite elements, and the cross-sections discretized into 10 layers.

Two analyses described in the literature are made here: a structure with steel columns and a composite beam (Structure 1) and a fully composite structural system (Structure 2). The displacement at the top of the right column is evaluated together with the incremental load to construct the equilibrium paths. Since in these two analyses composite beams were used without reinforcement in the negative moment region, it is proposed in this work to evaluate the gain of bearing capacity provided by including reinforcing bars in the slab. Structure 3 is then referred to as the frame with steel columns and an reinforced composite beam in the negative moment region while Structure 4 is referred to as the composite frame with an reinforced composite beam in the negative moment region.

For the steel, a yield strength f_y equal to 248.2 MPa is considered along with a Young's modulus taken as 200000 MPa. The concrete compressive strength characteristic, f_c, adopted is 16 MPa and the secant modulus is calculated relating f_c with strain ε_{ci} taken as -0.002. The actual strain was not allowed to exceed -0.0035, defined as ε_{cu}.

Figure 13 shows the load-displacement curves for the four cases described above. The runtimes measured from the start of the analysis until the time when the load limit was reached for the structures 1, 2, 3, and 4 were the following: 0.64s, 0.66s, 0.65s, and 0.73s. In the equilibrium paths obtained through the analysis via the CS-ASA, one can see in both analyses, a almost instant loss of stiffness of the structural system near the incremental load P equal to 60 kN. This fact is related to the first plastic hinge of the frame (Fig. 14) occurring in the beam near the junction with the right column. This portion concerns the effect of the negative moment. That is, the contribution of the concrete slab is practically null, since it has no longitudinal reinforcements. In this same figure it can be seen that only the beam has points in plastic and elastoplastic stages. Thus, it is concluded that encased I section in the columns does not significantly alter the bearing capacity of the structural system as a whole. The major contribution of filling the columns with concrete is amplifying these elements stiffness. The speed with which the plastification occurs is due to the constitutive relation adopted for the steel. With elastic-perfectly-plastic

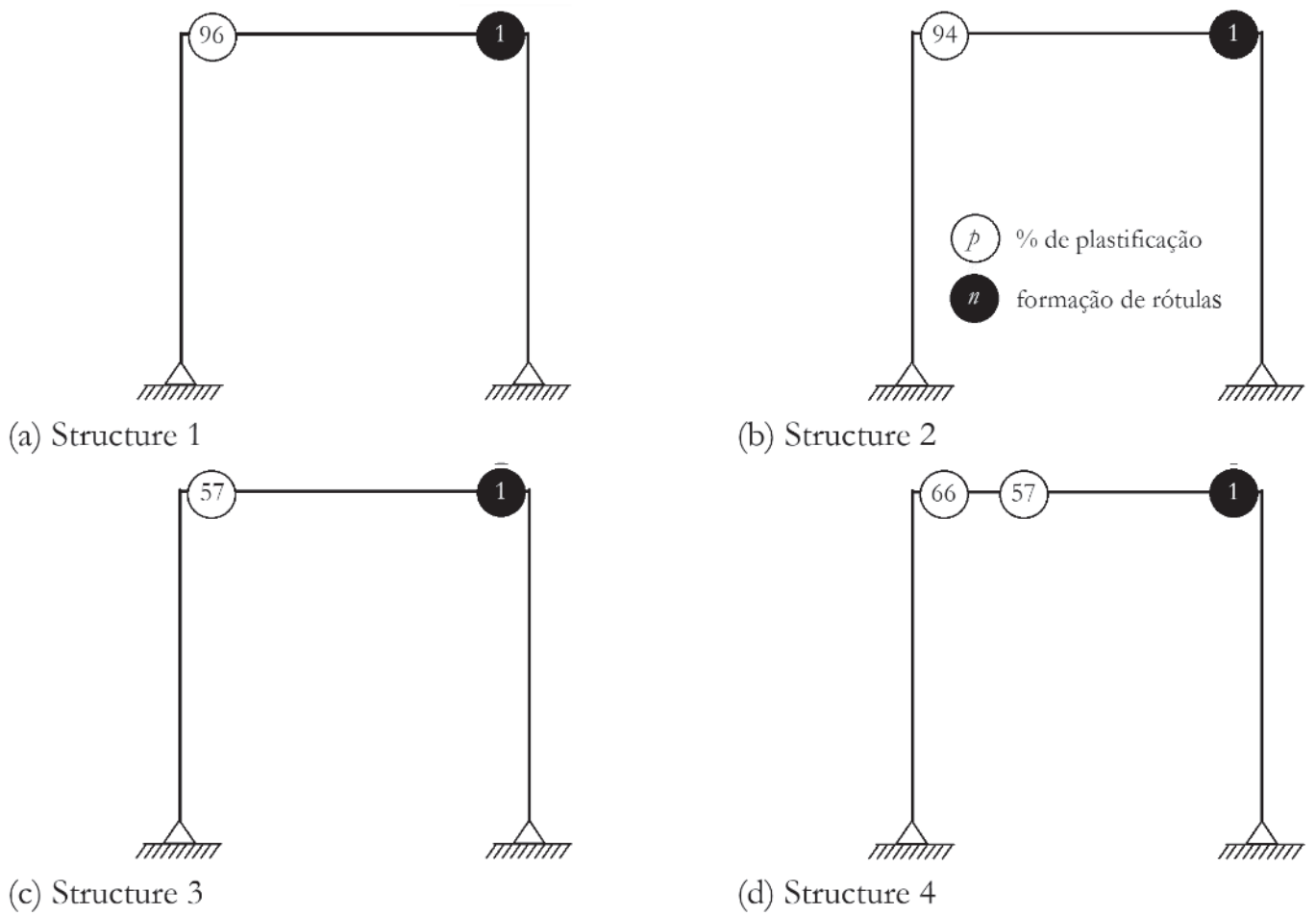

Figure 14
Plastic hinge formation sequence

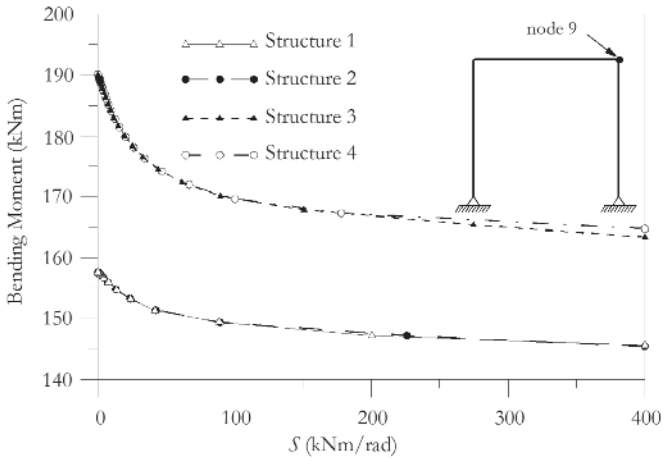

Figure 15
Degradation of the pseudo-spring flexural stiffness in node 9

behavior, the initial and full yield curves are very close, resulting in the reduction of the portion of the stiffness degradation (elastoplastic stage).

When one considers the reinforcing bars with diameter equal to 8 mm (f_{yr} = 400 MPa and E_b = 200 GPa) in the negative bending moment, it may be clearly noticed that there is a disappearance of the near instantaneous loss of stiffness under load P equal to 60 kN. The reinforcing bars inserted in the slab amplify the resistant bending moment, increasing the elastoplastic stage of the cross-section. Thus, the stiffness degradation is subtler if seen in the equilibrium path in Fig. 14. As a result, we see a gain of approximately 7% in the structure's load capacity (load limit P) as a whole. The percentage of plastification is shown in the unfilled circles. Figure 15 illustrates how, in relation to the bending moment, the stiffness degradations of the pseudo-springs occur in Node 9 of the structure.

The plastification starts when the ratio of moment x *S* ceases to be parallel with the horizontal axis, that is, when the section reaches the initial yield moment. When the stiffness *S* is zero, the full yield moment is attained. That is, the combination of internal forces lies on the full yield curve.

7. Conclusions

In this paper was presented a numerical formulation based on Refined Plastic Hinge Method Refined (RPHM) for advanced analysis of steel-concrete composite structures. In this context, was coupled to the CS-ASA program a general methodology to obtain the bearing capacity, the Strain Compatibility Method (SCM). The axial and flexural stiffness were determined through homogenization of the cross-section.

In SCM, the Newton-Raphson Method is used to determine the moment-curvature relationship. Its generality allows that, through the presented constitutive relations, steel or reinforced concrete sections subjected to a combination of axial force and bending moment, be also modeled. It was found in Section 6.1 that the use of the singularity of the stiffness matrix as stopping criterion of the construction of the moment-curvature relationship, adopted in this study, is consistent with strain domains used by Caldas [10]. In Figures 7 and 8 was seen that the consideration of the concrete tensile strength contribution added approximately 2% in the bearing capacity of composite sections under positive normal forces. In composite sections, there is a preponderant share of the steel section tensioned regions, since their behavior is treated as isotropic. Evaluation of composite elements considering the concentrated plasticity via RPHM also showed results consistent with the literature. In Sections 6.2 and 6.3 were evaluated standard composite elements under simple bending and compression, and in both cases the results were compared with data obtained in laboratory. In Tables 2 and 3 were highlighted, on average, good proximity between the numerical and experimental results. Furthermore, the low dispersion of the results from the average indicate the reliability of the analysis.

Figures 13a and 13b illustrate two simple frames behavior with the same geometry but different cross-sections for the columns. At first only steel vertical elements (columns) were considered, then the columns were completely encased with concrete. It is noticed that there was no great increase in limit load, which is defined by the composite beam. An important fact to be noted is that in the literature analyzes, the composite beam is not reinforced in the negative bending moment region. Thus, only the steel section works as a structural element. This fact associated with elastoplastic behavior used in this work, induce a loss of sharp system stiffness (plastification at the right end of the beam) when the load parameter is approximately 60 kN. It was then proposed in this paper the reinforcing bars insertion in the composite beam in the negative bending moment region. Thus, the reinforcing bars introduces an increase of bearing capacity in the critical section of the structural system, as illustrated in Fig. 14. This fact resulted in a 7% increase in the load limit of the structure and 17% in full yield bending moment of the beam in negative region, as illustrated in Fig. 15.

In addition, it should be noted the low execution time of the simulations carried out in Section 6 of this work. It was observed during the analysis that the formulation in question, in terms of runtime, showed a certain sensitivity for the initial load increment parameter. Very small values increase the runtime but improve the accuracy of the final response. This observation can also be made with regard to local and global mesh. Nevertheless, the examples presented here, it was found that a low refining rate of such meshes showed satisfactory results with respect to data in the literature. It is noteworthy that in Example 6.2 a discretization slightly more refined was used than in the other problems mentioned in Section 6. This can be explained by the level of refining required for the modeling of circular sections, since the layers generated in the discretization of the cross-section are rectangular, as illustrated in Fig. 5.

What has not been addressed in this work are the reinforced concrete elements the overall structural context. In fact, the methodology presented in terms of an analysis of the structure as a whole, does not allow a good evaluation of this type of structure. When considering that a section has flexural stiffness variation only when the internal forces reach the initial yield curve, it is assumed that every type of element initially presents a linear elastic behavior. As future stages of this research, we intend to eliminate this limitation

with the generalization of obtaining the axial and flexural stiffness, which will be taken directly from moment-curvature relationships in the two nodal points of the finite element. Thus, the use of the tangent modulus to provide greater accuracy analyzes. The behavior of composite elements with partial interaction and composite frames with semi-rigid connections will also be studied. In addition, it intends to extend the formulations and simulations to dynamic analysis of composite structures.

8. Acknowledgment

The authors would like to thank CAPES, CNPq, Fapemig, and UFOP for their support during the preparation of this work. Special thanks go to prof. John White for the editorial review of this text.

9. References

[1] COMITE EUROPEEN DE NORMALISATION. Design of composite steel and concrete structures part I: general rules and rules for buildings. – EUROCODE 4, Brussels, Belgium, 2004.

[2] AMERICAN INSTITUTE OF STEEL CONSTRUCTION. Specification for structural steel buildings, Chicago, USA, 2010.

[3] WENG, C.C., YEN, S.L. Comparisons of concrete-encased composite column strength provision of ACI code and AISC specifications. Engineering Structures, v.24, 2002; p.59-72.

[4] CHAN, S.L., CHUI, P.P.T. Non-linear static and cyclic analysis of steel frames with semi-rigid connections, Oxford: Elsevier, 2000, 336 p.

[5] SILVA, A.R.D. Sistema computacional para análises avançada estática e dinâmica de estruturas metálicas, Ouro Preto, 2009, Tese (doutorado) – Programa de Pós-graduação em Engenharia Civil, Universidade Federal de Ouro Preto, 322 p.

[6] FONG M., CHAN, S.L. Advanced analysis of steel-concrete composite beam-columns by refined plastic-hinge method. International Journal of Structural Stability and Dynamics, v.12, 2012.

[7] LEMES, Í.J.M. Análise avançada via RPHM de estruturas mistas de aço e concreto, Ouro Preto, 2009, Dissertação (mestrado) – Programa de Pós-graduação em Engenharia Civil, Universidade Federal de Ouro Preto, 101 p.

[8] CHEN, S., TENG, J.G., CHAN, S.L. Design of biaxially loaded short composite columns of arbitrary section. Journal of Structural Engineering, v.127, n.6, 2001; p.678-685.

[9] LIU, S.W., LIU, Y.P., CHAN, S.L. Advanced analysis of hybrid steel and concrete frames part 1: Cross-section analysis technique and second order analysis. Journal of Constructional Steel Research, v.70, 2012; p.326-336.

[10] CALDAS, R. B. Análise numérica de pilares mistos aço-concreto, Ouro Preto, 2004, Dissertação (mestrado) – Programa de Pós-graduação em Engenharia Civil, Universidade Federal de Ouro Preto, 200 p.

[11] CHIOREAN, C.G. A computer method for nonlinear inelastic analysis of 3d composite steel-concrete frame structures. Engineering Structures, v.57, 2013; p.125-152.

[12] LIU, S.W., LIU, Y.P., CHAN, S.L. Advanced analysis of hybrid steel and concrete frames part 2: Refined plastic hinge and advanced analysis. Journal of Constructional Steel Research, v.70, 2012; p.337-349.

[13] CHAN, S.L, Liu, S.W., LIU, Y.P. Advanced analysis of hybrid frames structures by refined plastic hinge approach. *In*: Steel and Composite Structures – Proceedings of 4th International Conference, 2010.

[14] YANG, Y.B., KUO, S.B. Theory & Analysis of Nonlinear Framed Structures, Singapore: Prentice Hall, 1994, 569 p.

[15] CHAN, S.L. Geometric and material nonlinear analysis of beam-columns and frames using the minimum residual displacement method. International Journal for Numerical Methods in Engineering, v.26, 1988; p.2657-2669.

[16] GALVÃO, A.S. Formulações não lineares de EF para análise de sistemas estruturais metálicos reticulados planos, Ouro Preto, 2000, Dissertação (mestrado) – Programa de Pós-graduação em Engenharia Civil, Universidade Federal de Ouro Preto, 168 p.

[17] LIEW, J., CHEN, H., SHANMUGAM, N. Inelastic analysis of steel frames with composite beams. Journal of Structural Engineering, v.127, 2001; p.194-202.

[18] BAZANT, Z.P., OH, B.H. Crack band theory for fracture of concrete. Materials and Structures, v.16, 1983; p.155-177.

[19] BRATINA, S., SAJE, M., PLANINC, I. On materially and geometrically non-linear analysis of reinforced concrete planar frames. International Journal of Solids and Structures, v.41, 2004; p.7181-7207.

[20] SFAKIANAKIS, M.G. Biaxial bending with axial force of reinforced, composite and repaired concrete sections of arbitrary shape by fiber model and computer graphics. Advances in Engineering Software, v. 33, 2002, p.227-242.

[21] NEOGI, P., SEN, H., CHAPMAN, J. Concrete-filled tubular steel columns under eccentric loading. The Structural Engineer, v. 47, 1969, p.187-195.

[22] AMERICAN CONCRETE INSTITUTE. Building code requirements for reinforced concrete. – ACI 318, 1995.

[23] LIU, D., GHO, W.M., YUAN, J. Ultimate capacity of high-strength rectangular concrete-filled steel hollow section stub columns. Journal of Constructional Steel Research, v. 59, 2003, p.1499-1515.

[24] IU, C.K., BRADFORD, M.A., CHEN, W.F. Second-order inelastic analysis of composite framed structures based on the refined plastic hinge method. Engineering Structures, v. 31, 2009, p.799-813.